

Quark Deconfinement Under the Influence of Strong Magnetic Fields

V. Dexheimer

Gettysburg College, Gettysburg, PA, USA

vantoche@gettysburg.edu

R. Negreiros

FIAS, Johann Wolfgang Goethe University, Frankfurt, DE

and

S. Schramm

FIAS, Johann Wolfgang Goethe University, Frankfurt, DE

Received _____; accepted _____

ABSTRACT

We study the effect of high magnetic fields on the particle population of neutron stars using an extended hadronic and quark SU(3) non-linear realization of the sigma model. In this model the degrees of freedom change naturally from hadrons to quarks as the density and/or temperature increases. The effects of high magnetic fields and anomalous magnetic moment (AMM) are visible in the macroscopic properties of the star, such as mass, adiabatic index, moment of inertia, and cooling curves.

Subject headings: stars: neutron — stars: magnetars — stars: interiors — stars: magnetic field — stars: evolution

1. Introduction

Magnetars are compact stars that have surface magnetic fields up to $10^{14} - 10^{15}$ G (Paczynski 1992; Ibrahim et al. 2004). Such fields can be estimated from observations of the star's period and period derivative. According to Virial theorem estimates, neutron stars could have a central magnetic field as large as 10^{18} or 10^{19} G in their interiors. The precise calculation of this limit is complicated, since all energies to be weighed with the magnetic energy (the one from matter and the gravitational one) also depend on the magnetic field. Furthermore, due to the asymmetry introduced by the magnetic field in the z-direction, the pressure becomes different in the parallel and perpendicular directions. In reality, depending on the magnitude of the magnetic field, the parallel pressure becomes much smaller than the perpendicular one, and in extreme cases, can go locally to zero. In ref. (Ferrer et al. 2010), as well as in our calculations, this limit was found to be around $10^{18} - 10^{19}$ G. Beyond this value strong instabilities can occur, which indicates that further investigation is necessary.

As the density increases towards the core of the star, hadronic matter can be deconfined into quark matter. Such a phase transition can be a sharp first order transition or include a mixed phase, depending on the surface tension between the phases. In this work we study the effect of the latter. One important question we will try to address is if the effects of strong magnetic fields in the deconfinement phase transition are strong enough to be observed. Other studies along this line are (Chakrabarty 1996; Bandyopadhyay et al. 1997; Rabhi et al. 2009; Paulucci et al. 2011). In order to do this in a realistic way we adopt as our microscopic model a chiral approach that includes hadronic as well as quark degrees of freedom in a unified description that was developed in (Dexheimer & Schramm 2010). Here, besides the analysis of the mass-radius diagram, we will extend our study to the adiabatic index and moment of inertia of the stars. Furthermore, we will, for the first time,

investigate the thermal evolution of highly magnetized hybrid stars, which will allow us to assess the effect of a high magnetic field on the cooling of the star.

2. The Model

Chiral sigma models are effective quantum relativistic models that describe hadrons interacting via meson exchange and, most importantly, are constructed from symmetry relations. They are constructed in a chirally invariant manner as the particle masses originate from interactions with the medium and, therefore, go to zero at high density/temperature. Adopting the nonlinear realization of the sigma model gives a significant improvement to the widely used linear sigma model (Papazoglou et al. 1998; Lenaghan et al. 2000) as it is in better agreement with nuclear physics results (Papazoglou et al. 1999; Bonanno & Drago 2009).

The Lagrangian density of the SU(3) non-linear sigma model in the mean field approximation constrained further by astrophysics data can be found in (Dexheimer & Schramm 2008). A recent extension of this model includes also quarks (Dexheimer & Schramm 2010). In this version, the degrees of freedom change due to the effective masses of the baryons and quarks. Their masses are generated by the scalar mesons (σ , isovector δ , strange ζ), except for a small explicit mass term M_0 and the term containing the field Φ , related to deconfinement in analogy with the Polyakov loop (Fukushima 2004). The baryon and quark masses are given by

$$M_B^* = g_{B\sigma}\sigma + g_{B\delta}\tau_3\delta + g_{B\zeta}\zeta + M_{0B} + g_{B\Phi}\Phi^2, \quad (1)$$

$$M_q^* = g_{q\sigma}\sigma + g_{q\delta}\tau_3\delta + g_{q\zeta}\zeta + M_{0q} + g_{q\Phi}(1 - \Phi), \quad (2)$$

where the values for the coupling constants can be found in (Dexheimer & Schramm 2010). With the increase of density/temperature, the σ field (non-strange chiral condensate)

decreases its value, causing the effective masses of the particles to decrease towards chiral symmetry restoration. The field Φ assumes non-zero values with the increase of temperature/density and, due to its presence in the baryons effective mass (Eq. (1)), suppresses their presence. On the other hand, the presence of the Φ field in the effective mass of the quarks, included with a negative sign (Eq. (2)), ensures that they will not be present at low temperatures/densities.

Both transitions, chiral symmetry restoration and deconfinement happen at the same density/temperature. Such a fact comes from the correlation of these quantities in the effective masses of the particles. The potential for Φ reads

$$U = (a_0 T^4 + a_1 \mu_B^4 + a_2 T^2 \mu_B^2) \Phi^2 + a_3 T_0^4 \log(1 - 6\Phi^2 + 8\Phi^3 - 3\Phi^4), \quad (3)$$

and allows the model to be used to study low, as well as high temperature environments, and make predictions for high-energy heavy-ion physics and comparisons with lattice QCD results (see (Dexheimer & Schramm 2010) for details).

3. Inclusion of Magnetic Field

In order to have a more detailed description of neutron stars, we include magnetic fields that, while being in the z-direction, are not constant. The effective magnetic dipole field B^* increases with baryonic chemical potential going from a surface value of $B_{surf} = 69.25 \text{ MeV}^2 = 10^{15} \text{ G}$ to a central value B_c

$$B^* = B_{surf} + B_c [1 - e^{b(\frac{\mu_B - 939}{939})}]. \quad (4)$$

In this way, there is no discontinuity in the magnetic field or in the increase of the magnetic field at the phase transition. Such an unphysical discontinuity would be present if we had chosen the effective magnetic field to be a function of baryonic density, as is usually done.

The constant b is chosen to reproduce (in the absence of quarks) the effective magnetic field curve as a function of density from (Bandyopadhyay et al. 1997; Mao et al. 2003). As can be seen in Fig 1, even with the use of extremely high central magnetic fields (recall that using Gaussian natural units $1 \text{ MeV}^2 = 1.44 \times 10^{13} \text{ G}$), the values for the effective magnetic fields only become extreme at very high baryonic chemical potentials that correspond to the inner core of the star. Such a dependence prevents effects like the spontaneous creation of electron-positron pairs in the star (Schwinger 1951).

The magnetic field in the z-direction forces the eigenstates in the x and y directions of the charged particles to be quantized into Landau levels ν

$$E_{i\nu s}^* = \sqrt{k_{z_i}^2 + \left(\sqrt{m_i^{*2} + 2\nu|q_i|B^*} - s_i\kappa_i B^* \right)^2}, \quad (5)$$

where k_i is the fermi momentum, q_i the charge and s_i the spin of each baryon or quark. The last term comes from the anomalous magnetic moment (AMM) of the particle that splits the energy levels with respect to the alignment/anti-alignment of the spin with the magnetic field. The AMM also modifies the energy levels of the uncharged particles

$$E_{i s}^* = \sqrt{k_i^2 + (m_i^{*2} - s_i\kappa_i B^*)^2}. \quad (6)$$

The constants κ_i determine the tensorial coupling strength of baryons with the electromagnetic field tensor and have values $\kappa_p = 1.79$, $\kappa_n = -1.91$, $\kappa_\Lambda = -0.61$, $\kappa_\Sigma^+ = 1.67$, $\kappa_\Sigma^0 = 1.61$, $\kappa_\Sigma^- = -0.38$, $\kappa_\Xi^0 = -1.25$, $\kappa_\Xi^- = 0.06$. The sign of κ_i determines the preferred orientation of the spin with the magnetic field. The sum over the Landau levels ν runs up to a maximum value, beyond which the momentum of the particles in the z-direction would be imaginary

$$\nu_{max} = \frac{E_{i s}^{*2} + s_i\kappa_i B^* - m_i^{*2}}{2|q_i|B^*}. \quad (7)$$

We choose to include in our calculations the AMM effect for the hadrons only, since the coupling strength of the particles κ_i depends on the corresponding magnetic moment,

that up to now is not fully understood for the quarks. Furthermore, it is stated in Ref. (Weinberg 1990), that quarks in the constituent quark model have no anomalous magnetic moment. For calculations including AMM effects for the quarks see (Chakrabarty 1996; Suh et al. 2001; Perez Martinez et al. 2005; Felipe et al. 2008). The AMM for the electrons is also not taken into account as its effect is negligibly small. The AMM removes the spin degeneracy of the particles and their energy levels are further split in two levels each, which increases even more the particle chemical potentials.

As can be seen in Fig. 2, a phase transition (chiral symmetry restoration and deconfinement) which is of first order at zero or small temperatures is delayed with the inclusion of high magnetic field. This effect is due to a stronger stiffening of the hadronic part of the EOS (as the magnetic field increases). It is important to notice that at very low densities, the hadronic EOS of non-interacting matter gets softer in the presence of high magnetic field, in agreement with (Broderick et al. 2000, 2002) and many other papers. In our case this effect is smaller because the magnetic field is only large at high densities. The EOS is shown in Fig. 3 for the case in which global charge neutrality is allowed and a mixed phase appears. We do not show the pure quark phase part, since in this model it is present only at very high densities that cannot be reached in the interior of the neutron star.

The delay on the phase transition is further increased when the anomalous magnetic moment is considered, as it only affects the hadronic phase rendering its EOS stiffer (due an increase in the chemical potential of the baryons). If global charge neutrality is assumed, the location of the mixed phase does not change substantially, except for the highest magnetic field considered with AMM, when the entire mixed phase is pushed to higher chemical potentials.

Fig. 4 shows the baryonic density of fermions (quark number densities are divided by 3). In the mixed phase the hadrons disappear smoothly and the quarks appear smoothly. The

hyperons, in spite of being included in the calculation, are suppressed by the appearance of the quark phase. Only a very small amount of Λ baryons appear right before the phase transition. The density of electrons and muons is significant in the hadronic phase but not in the quark phase. The reason for this behavior is that, because the down and strange quarks are also negatively charged, there is no necessity for the presence of electrons to maintain charge neutrality, and only a small amount of leptons remains to ensure beta equilibrium. The strange quarks appear after the other quarks and do not make substantial changes in the system.

The largest possible change in the population is shown in Fig. 5, for $B_c = 1 \times 10^6 \text{ MeV}^2$ with AMM. The wiggles in the charge particle densities come from the Landau levels, more precisely when the Fermi energy of the particles cross the discrete threshold of a Landau level. The charged particles are enhanced (as their chemical potentials increase with B), which is especially visible in the amount of electrons in the quark phase. The remaining hyperons are even more suppressed due to the increase in the proton density.

4. Macroscopic Properties

A key point of this investigation is to determine whether the changes due to the presence of magnetic field are strong enough to affect observable properties of the stars. To answer this question, we are going to analyze the adiabatic index, moment of inertia, mass-radius diagram and thermal evolution for different magnetic fields.

4.1. Adiabatic Index

We begin with the adiabatic index (Fig. 6). The discontinuities in the $B = 0$ curve show the appearance of the Λ 's and the beginning of the mixed phase. The extra peaks in

the $B_c = 1 \times 10^6 \text{ MeV}^2$ with AMM curve show the Landau level thresholds that also can be seen in the population plot. As pointed out in (Ryu et al. 2011), these rapid changes in the pressure can cause instabilities in the star that might cause star-quakes, glitches and giant flares.

4.2. Moment of Inertia

In Fig. 7 we show the moment of inertia as function of radius for several of the investigated stellar sequences. We see that for the maximum central magnetic field considered ($1 \times 10^6 \text{ MeV}^2$), there is an increase of about 10% from the unmagnetized case (for the maximum mass star). If the anomalous magnetic moment is not considered, the increase is more modest ($\sim 6\%$). This result indicates that if the magnetic field of the object is changing, the moment of inertia will be modified, which might affect the spin evolution of the object, and might allow one to make a connection between AXP emission and glitches (see discussion in (Ryu et al. 2011)). For lower central magnetic fields, the moments of inertia are almost the same as in the non-magnetized case.

4.3. Mass radius diagram

The possible neutron star masses and radii are calculated by solving the Tolman-Oppenheimer-Volkoff equations (Tolman 1939; Oppenheimer & Volkoff 1939). In Fig. 8, besides our equation of state for the core, a separate equation of state was used for the crust (Baym et al. 1971). The maximum mass supported against gravity is higher for higher magnetic fields and even higher when the AMM is included. It is important to note that in this model pure quark matter only appears at very high densities, that correspond to the unstable branch of the mass-radius diagram. Thus, only hadronic and “mixed” matter

appear in the star.

So far, the magnetic field pressure was not considered and only the influence of the magnetic field on the energy levels of the particles was taken into account. The problem in including the magnetic pressure is that it has different values in the directions parallel and perpendicular to the field, as can be seen in the electromagnetic energy-momentum tensor

$$T^{\mu\nu} = \frac{1}{4\pi} \begin{pmatrix} \frac{1}{2}B^{*2} & 0 & 0 & 0 \\ 0 & \frac{1}{2}B^{*2} & 0 & 0 \\ 0 & 0 & \frac{1}{2}B^{*2} & 0 \\ 0 & 0 & 0 & -\frac{1}{2}B^{*2} \end{pmatrix}, \quad (8)$$

where the first term is related to the energy density and the other three to the pressure in the x , y and z directions. This problem was pointed out in many papers as (Chaichian et al. 2000; Perez Martinez et al. 2003; Perez Martinez et al. 2005; Felipe et al. 2008; Perez Martinez et al. 2008; Ferrer et al. 2010; Orsaria et al. 2011; Paulucci et al. 2011). In these papers, there is also a term coming from the magnetic dipole interaction, which is linear in B and is therefore subleading at high magnetic fields. A consistent inclusion of the macroscopic magnetic pressure would require 2D calculations, which currently is not available. Most calculations consider the pressure term to be positive in all directions or negative in all directions. It was pointed out by (Bandyopadhyay et al. 1997; Sinha & Mukhopadhyay 2010) that negative pressure in all directions constrains the maximum values that can be used for the magnetic field to lower values. In our case, $B_c = 5 \times 10^5 \text{ MeV}^2$ would already cause such instability at very high densities. A third option, suggested by (Bednarek et al. 2003) uses, as monopole approximation of the energy-momentum tensor, the average between the three pressures and adds $+B^2/24\pi$ for the magnetic pressure in all directions. We show the difference caused by either choosing the pressure to be positive in all directions or using the average pressure in the mass-radius diagram. Obviously the first case is unphysical as the magnetic pressure dominates over any

other contribution. We speculate that the correct value would be close to the third option that uses the average of the pressures in different directions, but any more precise statement requires the use of axisymmetric TOV equations, as was already pointed by (Paulucci et al. 2011). Work along this line is ongoing and will allow for a more exact estimate of the increase of the star mass based on the magnitude of the magnetic field of the magnetar.

4.4. Thermal Evolution

We now turn our attention to the thermal evolution of hybrid stars, whose microscopic composition is given by the model described in this paper. The cooling of compact stars is given by the thermal balance and thermal energy transport equation ($G = c = 1$) (Weber 1999)

$$\frac{\partial(l e^{2\phi})}{\partial m} = -\frac{1}{\rho\sqrt{1-2m/r}} \left(\epsilon_\nu e^{2\phi} + c_v \frac{\partial(T e^\phi)}{\partial t} \right), \quad (9)$$

$$\frac{\partial(T e^\phi)}{\partial m} = -\frac{(l e^\phi)}{16\pi^2 r^4 \kappa \rho \sqrt{1-2m/r}}. \quad (10)$$

In Eqs. (9)–(10) the structure of the star is given by the variables r , $\rho(r)$, e^ϕ and $m(r)$, that represent the radial distance, the energy density, the metric function, and the stellar mass, respectively. The thermal variables are given by the temperature $T(r, t)$, luminosity $l(r, t)$, neutrino emissivity $\epsilon_\nu(r, T)$, thermal conductivity $\kappa(r, T)$, and specific heat $c_v(r, T)$. The boundary conditions of (9) and (10) are determined by the luminosity at the stellar center and at the surface. The luminosity vanishes at the stellar center since there is no heat flux there. At the surface, the luminosity is defined by the relationship between the mantle temperature and the temperature outside of the star (Gudmundsson et al. 1982, 1983; Page et al. 2006; Blaschke et al. 2000). For the hadronic phase, we have considered the following neutrino emission processes: direct Urca, modified Urca and bremsstrahlung processes; whereas for the quark phase, the processes taken into account are the quark

direct Urca, quark modified Urca, and quark bremsstrahlung processes. Details about the emissivities of such processes can be found in references (Yakovlev et al. 2001; Iwamoto 1982). The specific heat of the hadrons is the usual specific heat of fermions, as described in (Page et al. 2004). As for the quarks, we use the expression for the specific heat calculated in (Iwamoto 1982). The thermal conductivity for the hadronic and quark matter were calculated, respectively in (Flowers & Itoh 1981; Haensel 1991), and in this work we follow the results presented in these references.

We have calculated the cooling for magnetized hybrid stars (with anomalous magnetic moment of the hadrons included) for three different masses: 1.1, 1.4 and 1.93 M_{\odot} . For each hybrid star mass we considered three values for the magnetic field ($1 \times 10^5, 5 \times 10^5, 1 \times 10^6$ MeV²). In addition to that we have also considered the effect of including the magnetic field pressure in the EoS.

The cooling of 1.1 M_{\odot} stars is shown in Fig. 9. One can see that in this case the star exhibits a slow cooling, which agrees relatively well with the observed data. Furthermore, we can also conclude that in this case the magnetic field has no substantial effect on the thermal evolution of the object, and neither does the inclusion of the magnetic pressure term in the EoS.

The situation is similar for stars with higher masses, as can be seen in Figs. 10 and 11, which show the thermal evolution of stars with 1.4 and 1.93 M_{\odot} , respectively. We see that in this case the modifications introduced by the magnetic field in the composition are not enough to alter the cooling (as was the case for lower mass stars). This picture changes, however, if one introduces the effect of the magnetic pressure. As shown in Figs. 10 and 11, the extra $B^{*2}/8\pi$ leads to slow cooling of a star that would otherwise exhibit fast cooling. The reason for this lies in the fact that adding an extra source of pressure stiffens the EoS. Hence, stars with higher masses possess smaller central densities and, therefore,

smaller proton fractions. The small proton fraction will hinder the otherwise present direct Urca process, thus leading to a slow cooling. The results for the inclusion of the magnetic pressure of $B^{*2}/24\pi$ are qualitatively the same. In this case, however, the stiffening of the EoS is more mild, and thus the effect is only appreciable for moderate masses, as seen in Fig. 10, where the thermal evolution is the same as for the magnetic pressure of $B^{*2}/8\pi$. For the $1.93 M_{\odot}$ star we see that the stiffening of the EoS is not enough to hinder the direct Urca process completely, and cooling of neutron stars with magnetic pressure of $B^{*2}/24\pi$ is only slightly slower.

5. Conclusions

To model magnetars, we use an effective model that includes hadronic and quarks degrees of freedom. As the density increases, the order parameters signal the deconfinement and chiral symmetry phase transitions, which happen more towards the center of the star for higher magnetic fields. The stiffness of the EOS, and the consequent star masses, depend on the chosen central magnetic field. It is clear that a higher B_c allows for more massive stars, but the quantitative analysis of how more massive the star can become requires the use of a 2D solution of Einstein's equations which takes into account the breaking of spherical symmetry by the magnetic field. Efforts along this line are currently being pursued. In addition to the effect on the mass-radius relationship, in this work we have shown that the presence of high magnetic fields can result in peaks in the adiabatic index and can modify the star's moment of inertia.

In our work we introduce an expression for the effective magnetic field B^* that increases with baryonic chemical potential, and therefore avoids a discontinuity in the phase transition region. This allows B^* to increase smoothly from a surface value up to a chosen central one (B_c). Furthermore, our investigation indicates that the composition changes, introduced

by the magnetic field, are not high enough to alter the thermal evolution of hybrid stars. We have found, however, that by including the magnetic pressure ($B^{*2}/8\pi$), the resulting stiffening of the EoS allows for stars with higher masses (1.4–1.93 M_{\odot}) leading to a slower cooling, which is in better agreement with the observed data. This is an important result, which indicates that one needs to understand better how to introduce the macroscopic pressure correctly into the structure of the star. We are cautious in interpreting these results, since the appropriate treatment of both the structure, and the thermal evolution of stars with such high magnetic fields would require a full two-dimensional study. We will save this investigation for a future work, as it seems clear to us that the effect of the magnetic pressure on the structure and thermal evolution might be substantial.

Subsequently, we would like to expand our study to finite temperature, in order to have a complete phase diagram (temperature as a function of baryonic chemical potential) for high magnetic field. A phase diagram for $T = 0$ was already constructed using the extended non-linear realization of the SU(3) sigma model in (Dexheimer & Schramm 2010). Such an analysis is important, since it connects the physics at high temperature and small densities, like the one created in heavy ion collisions, with the physics inside neutron stars. Such a finite- B phase diagram was already constructed by (Chakrabarty 1996) but we believe that we can give further insight into the matter with our model, since it also includes chiral symmetry restoration and allows for a smooth chiral and deconfinement crossover transition at small densities.

We are grateful to Constanca Providencia, Milva Orsaria, Fridolin Weber, Debora Menezes and Aurora Perez Martinez for the fruitful discussions on the matter of strong magnetic fields. R. N. acknowledges financial support from the LOEWE program HIC for FAIR.

REFERENCES

- Bandyopadhyay, D., Chakrabarty, S., & Pal, S. 1997, *Phys. Rev. Lett.*, 79, 2176
- Baym, G., Pethick, C., & Sutherland, P. 1971, *Astrophys.J.*, 170, 299
- Bednarek, I., Brzezina, A., Manka, R., & Zastawny-Kubica, M. 2003, *Nucl.Phys.*, A716, 245
- Blaschke, D., Klahn, T., & Voskresensky, D. 2000, *The Astrophysical Journal*, 533, 406412
- Bonanno, L., & Drago, A. 2009, *Phys. Rev.*, C79, 045801
- Broderick, A., Prakash, M., & Lattimer, J. M. 2000
- Broderick, A. E., Prakash, M., & Lattimer, J. M. 2002, *Phys. Lett.*, B531, 167
- Chaichian, M., Masood, S. S., Montonen, C., Perez Martinez, A., & Perez Rojas, H. 2000, *Physical Review Letters*, 84, 5261
- Chakrabarty, S. 1996, *Phys. Rev.*, D54, 1306
- Dexheimer, V., & Schramm, S. 2008, *Astrophys. J.*, 683, 943
- Dexheimer, V. A., & Schramm, S. 2010, *Phys. Rev.*, C81, 045201
- Felipe, R. G., Martinez, A. P., Rojas, H. P., & Orsaria, M. 2008, *Phys. Rev.*, C77, 015807
- Ferrer, E. J., de la Incera, V., Keith, J. P., Portillo, I., & Springsteen, P. P. 2010, *Phys. Rev.*, C82, 065802
- Flowers, E., & Itoh, N. 1981, *The Astrophysical Journal*, 250, 750
- Fukushima, K. 2004, *Phys. Lett.*, B591, 277
- Gudmundsson, E. H., Pethick, C. J., & Epstein, R. I. 1982, *The Astrophysical Journal*, 259,

- Gudmundsson, E. H., Pethick, C. J., & Epstein, R. I. 1983, *The Astrophysical Journal*, 272, 286
- Haensel, P. 1991, *Nuclear Physics B - Proceedings Supplements*, 24, 23
- Ibrahim, A. I., et al. 2004, *AIP Conf. Proc.*, 714, 294
- Iwamoto, N. 1982, *Annals of Physics*, 141, 1
- Lenaghan, J. T., Rischke, D. H., & Schaffner-Bielich, J. 2000, *Phys. Rev.*, D62, 085008
- Mao, G.-J., Iwamoto, A., & Li, Z.-X. 2003, *Chin. J. Astron. Astrophys.*, 3, 359
- Oppenheimer, J., & Volkoff, G. 1939, *Phys.Rev.*, 55, 374
- Orsaria, M., Ranea-Sandoval, I. F., & Vucetich, H. 2011, *Astrophys. J.*, 734, 41
- Paczynski, B. 1992, *Acta Astron.*, 42, 145
- Page, D., Geppert, U., & Weber, F. 2006, *Nuclear Physics A*, 777, 497
- Page, D., Lattimer, J., Prakash, M., & Steiner, A. W. 2004, *The Astrophysical Journal Supplement Series*, 155, 623
- Papazoglou, P., Schramm, S., Schaffner-Bielich, J., Stoecker, H., & Greiner, W. 1998, *Phys. Rev.*, C57, 2576
- Papazoglou, P., et al. 1999, *Phys. Rev.*, C59, 411
- Paulucci, L., Ferrer, E. J., de la Incera, V., & Horvath, J. E. 2011, *Phys. Rev.*, D83, 043009
- Perez Martinez, A., Perez Rojas, H., & Mosquera Cuesta, H. 2008, *Int. J. Mod. Phys.*, D17, 2107

- Perez Martinez, A., Perez Rojas, H., Mosquera Cuesta, H. J., Boligan, M., & Orsaria, M. G. 2005, *Int. J. Mod. Phys.*, D14, 1959
- Perez Martinez, A., Perez Rojas, H., & Mosquera Cuesta, H. J. 2003, *European Physical Journal C*, 29, 111
- Rabhi, A., Pais, H., Panda, P. K., & Providencia, C. 2009, *J. Phys.*, G36, 115204
- Ryu, C.-Y., Cheoun, M.-K., Kajino, T., Maruyama, T., & Mathews, G. J. 2011
- Schwinger, J. S. 1951, *Phys. Rev.*, 82, 664
- Sinha, M., & Mukhopadhyay, B. 2010
- Suh, I.-S., Mathews, G. J., & Weber, F. 2001
- Tolman, R. C. 1939, *Phys.Rev.*, 55, 364
- Weber, F. 1999, *Pulsars as astrophysical laboratories for nuclear and particle physics*, 1st edn. (Bristol: Institute of Physics)
- Weinberg, S. 1990, *Phys. Rev. Lett.*, 65, 1181
- Yakovlev, D. G., Kaminker, A. D., Gnedin, O. Y., & Haensel, P. 2001, *Physics Reports*, 354, 1

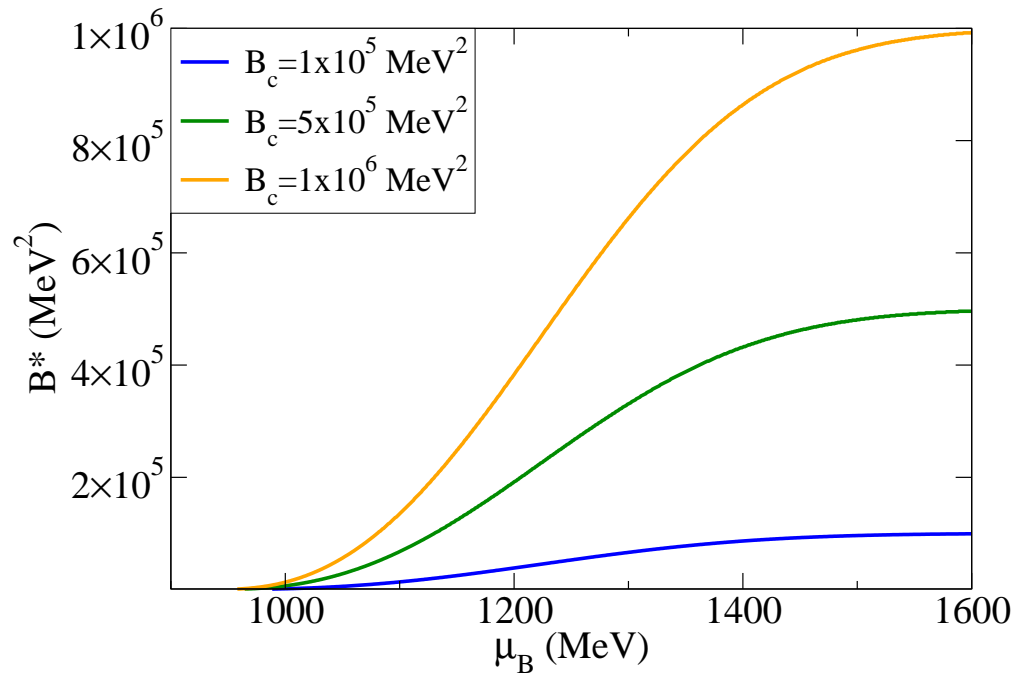


Fig. 1.— (Color online) Effective magnetic field as a function of baryonic chemical potential shown for different central magnetic fields.

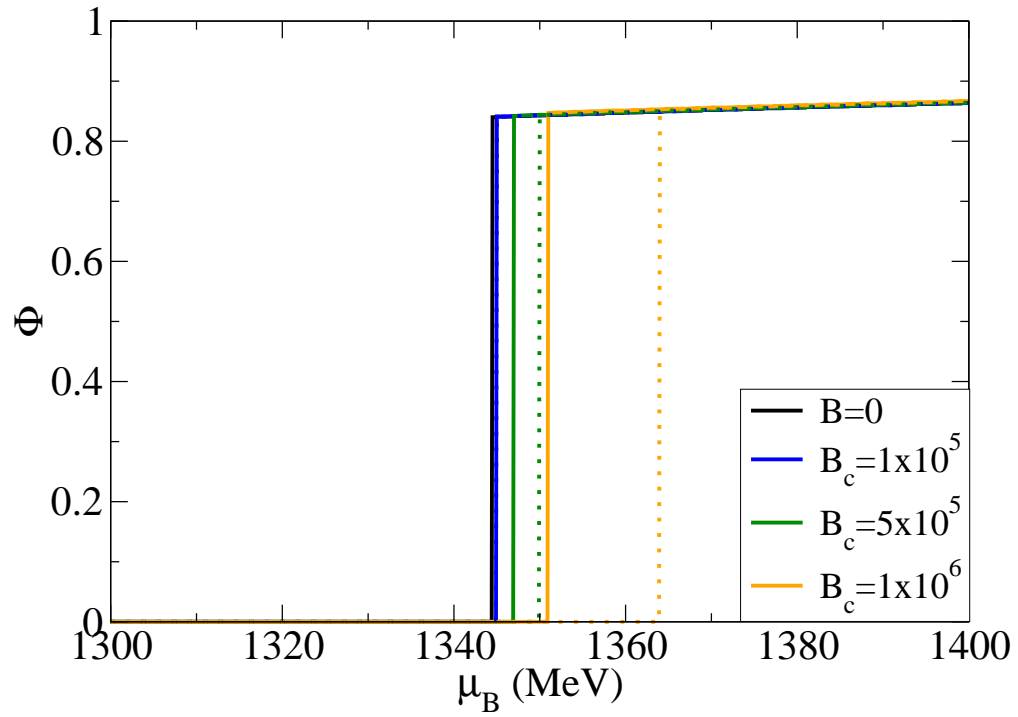


Fig. 2.— (Color online) Deconfinement order parameter as a function of baryonic chemical potential imposing local charge neutrality shown for different central magnetic fields. Dotted lines include AMM.

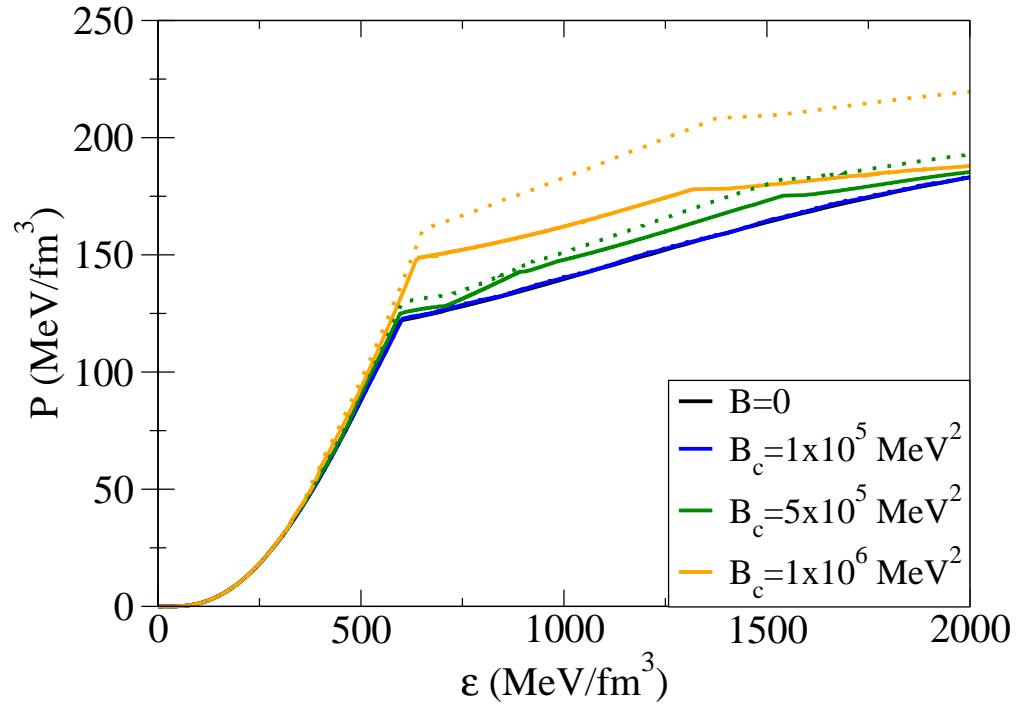


Fig. 3.— (Color online) Equation of State (pressure of matter as a function of energy density of matter) assuming global charge neutrality for different central magnetic fields. Dotted lines include AMM.

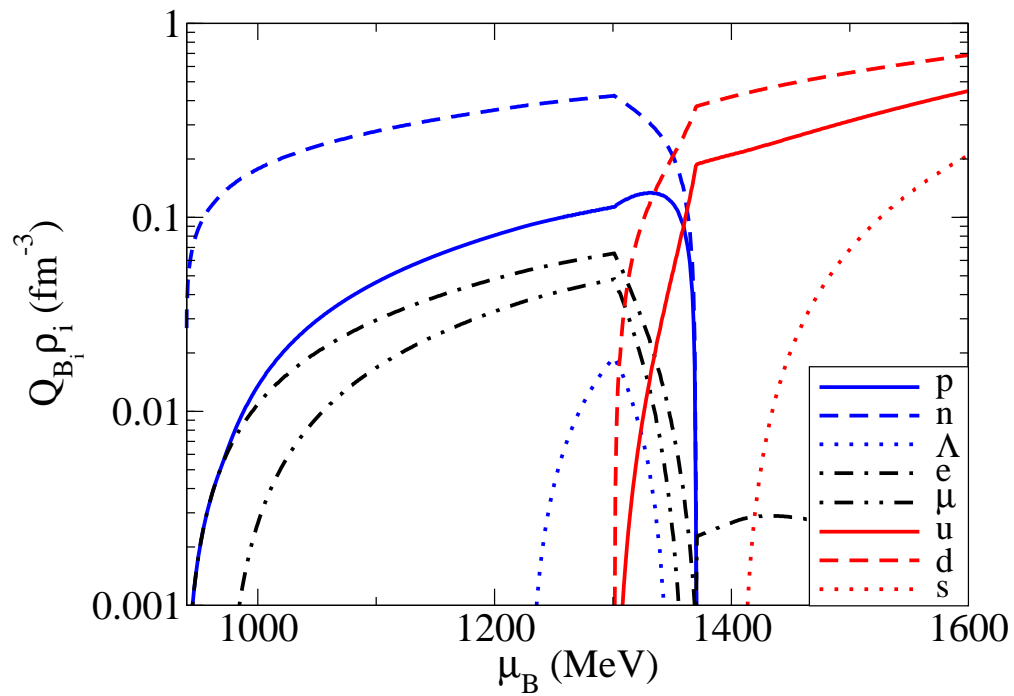


Fig. 4.— (Color online) Particle densities as a function of baryonic chemical potential assuming global charge neutrality for $B=0$.

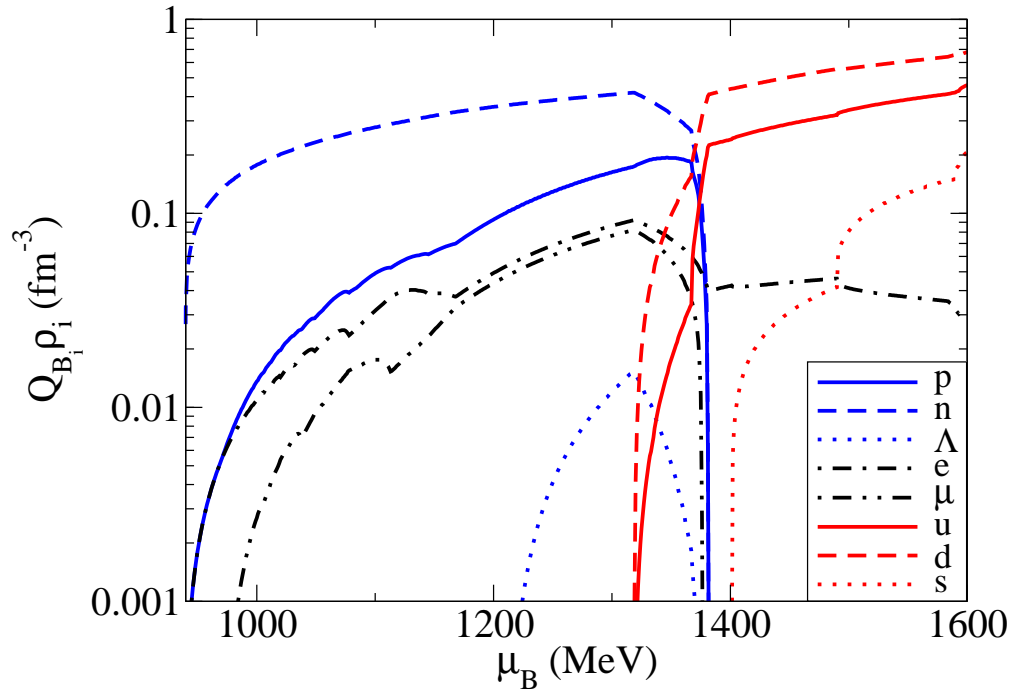


Fig. 5.— (Color online) Particle densities as a function of baryonic chemical potential assuming global charge neutrality for $B_c = 10^6 \text{ MeV}^2$ including AMM.

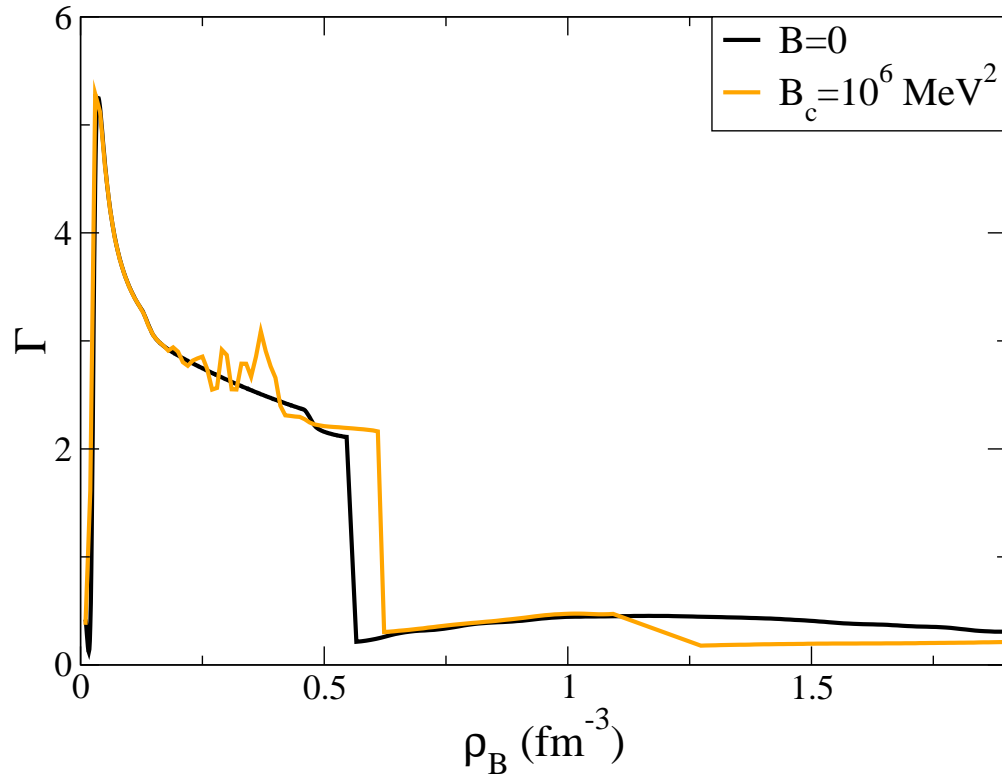


Fig. 6.— (Color online) Adiabatic index as a function of baryonic density for $B = 0$ and $B_c = 10^6 \text{ MeV}^2$ including AMM.

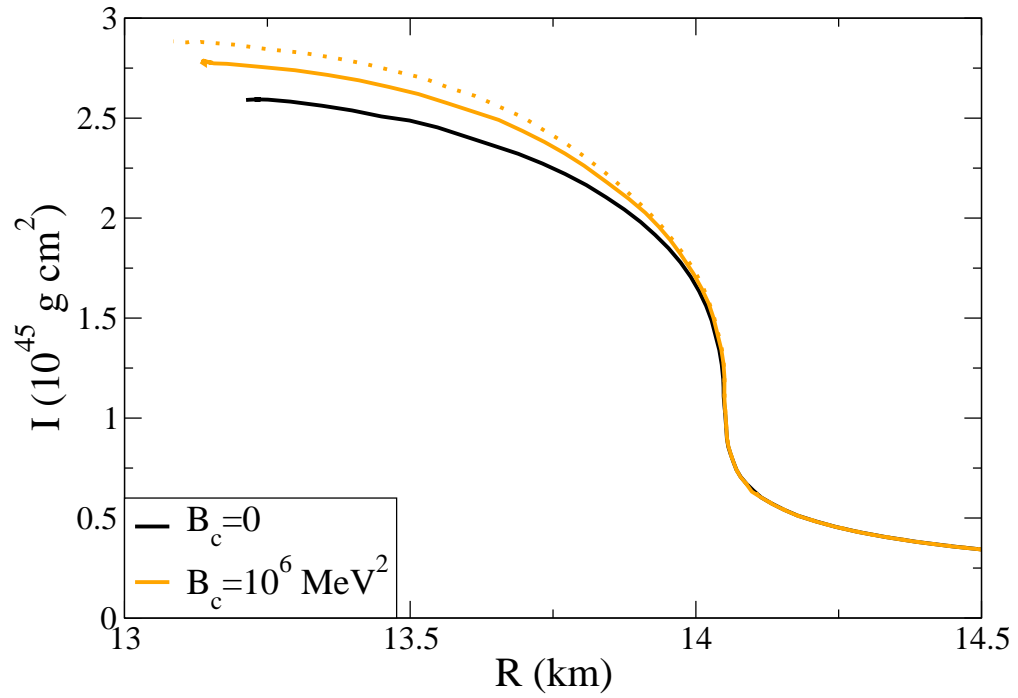


Fig. 7.— (Color online) Moment of inertia as a function of radius for $B = 0$ and $B_c = 10^6 \text{ MeV}^2$. Dotted line includes AMM.

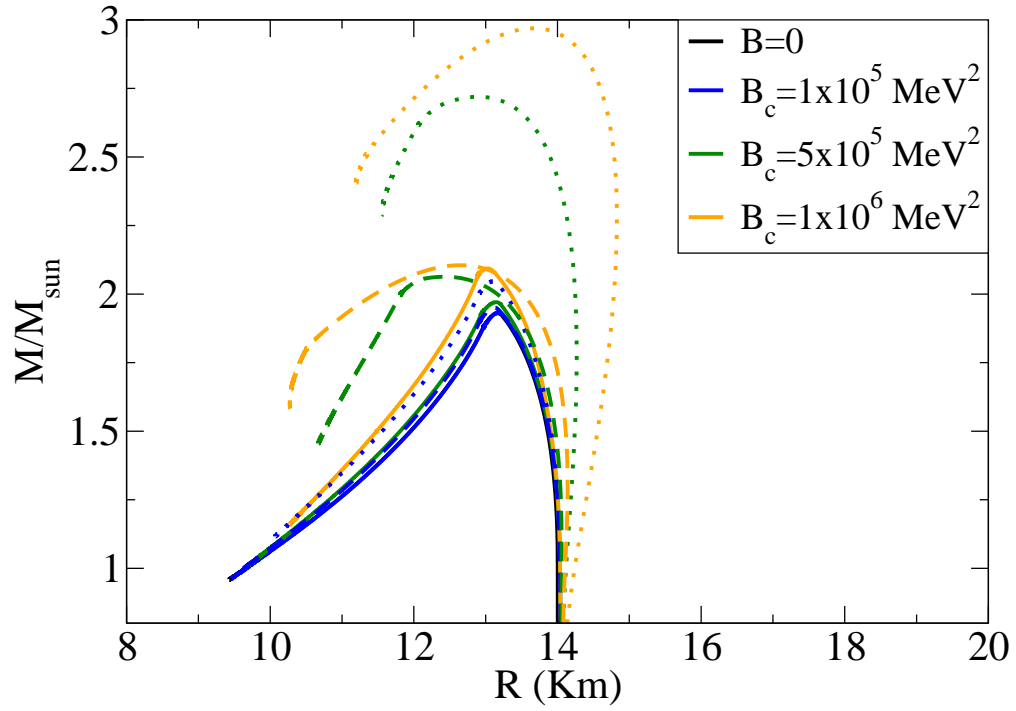


Fig. 8.— (Color online) Mass-radius diagram shown for different central magnetic fields including AMM. The dashed and dotted lines have the extra magnetic pressure term of $B^{*2}/24\pi$ and $B^{*2}/8\pi$, respectively, added to the total pressure.

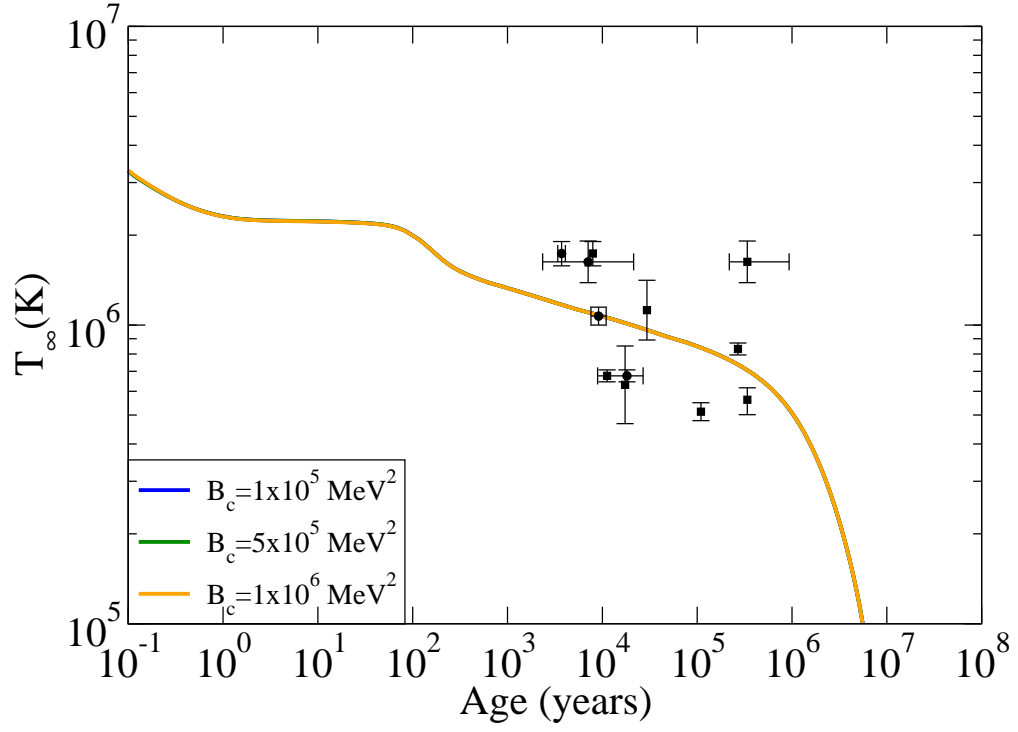


Fig. 9.— (Color online) Cooling curves for a $1.1 M_\odot$ mass star in the presence of different central magnetic fields including AMM. The dashed and dotted lines include the extra magnetic pressure term of $B^{*2}/24\pi$ and $B^{*2}/8\pi$, respectively. All curves overlap.

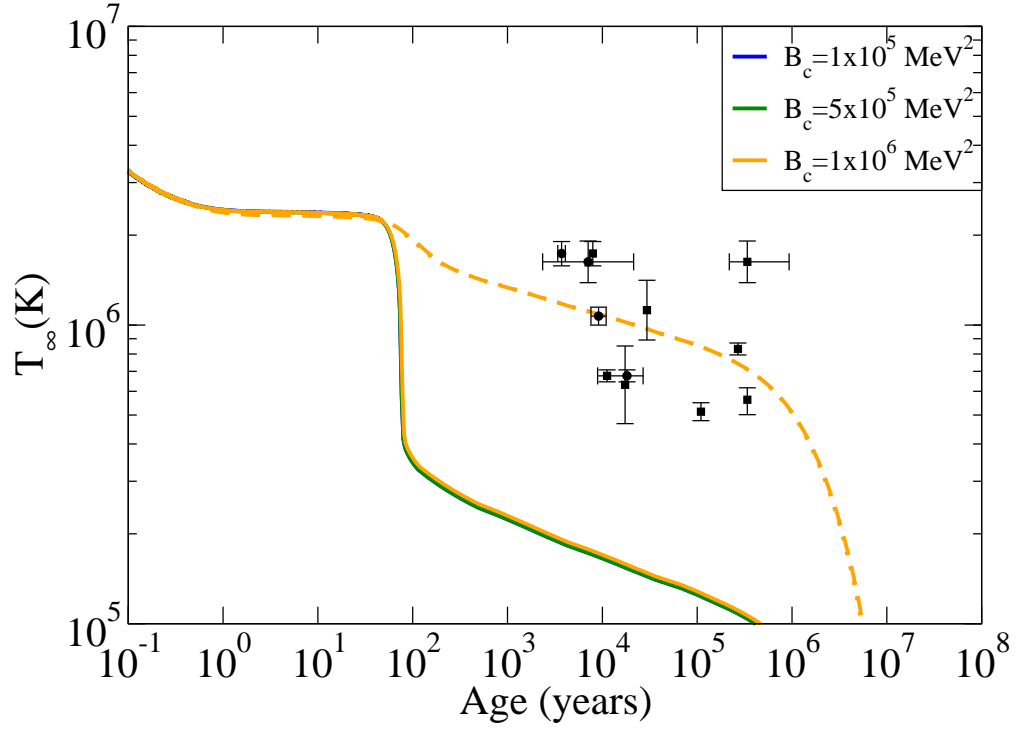


Fig. 10.— (Color online) Cooling curves for a $1.4 M_\odot$ mass star in the presence of different central magnetic fields including AMM. The dashed and dotted lines include the extra magnetic pressure term of $B^{*2}/24\pi$ and $B^{*2}/8\pi$, respectively. These two curves overlap.

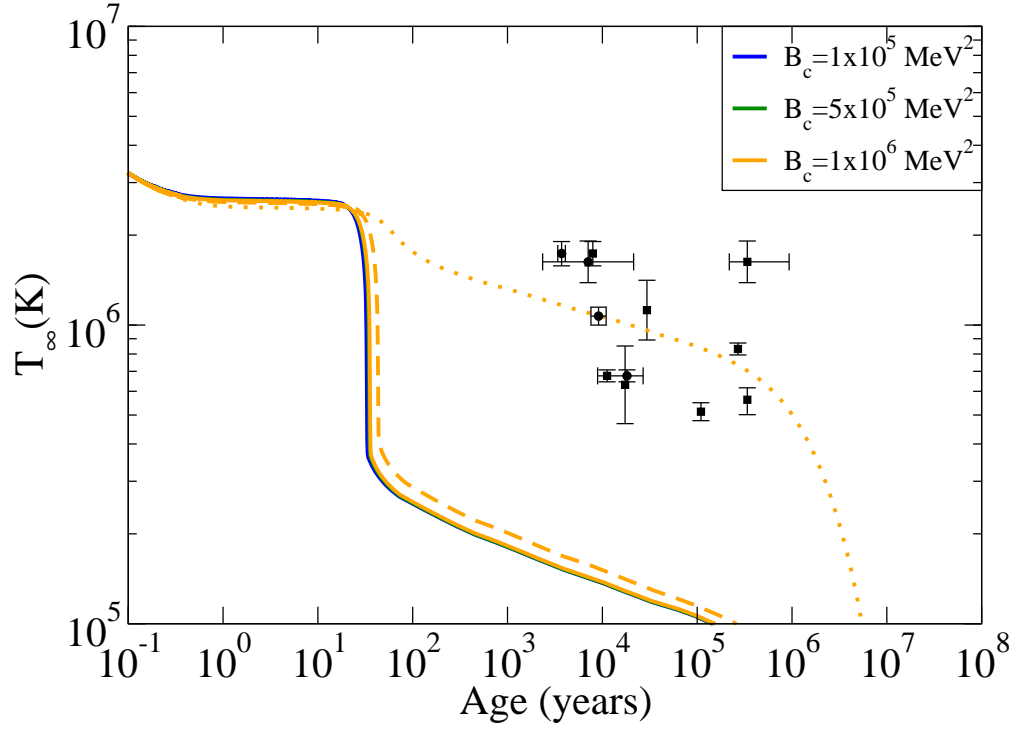


Fig. 11.— (Color online) Cooling curves for a $1.93 M_\odot$ mass star in the presence of different central magnetic fields including AMM. The dashed and dotted lines have extra magnetic pressure term added to the total pressure of $B^{*2}/24\pi$ and $B^{*2}/8\pi$, respectively.